

Provided for non-commercial research and education use.
Not for reproduction, distribution or commercial use.



This article appeared in a journal published by Elsevier. The attached copy is furnished to the author for internal non-commercial research and education use, including for instruction at the authors institution and sharing with colleagues.

Other uses, including reproduction and distribution, or selling or licensing copies, or posting to personal, institutional or third party websites are prohibited.

In most cases authors are permitted to post their version of the article (e.g. in Word or Tex form) to their personal website or institutional repository. Authors requiring further information regarding Elsevier's archiving and manuscript policies are encouraged to visit:

<http://www.elsevier.com/authorsrights>



Contents lists available at ScienceDirect

Journal of Alloys and Compounds

journal homepage: www.elsevier.com/locate/jalcom

Mesoporous nanonickel oxide: Anode with good initial discharge capacity and efficiency in lithium ion batteries at 1 C rate



Emad M. Masoud*

Chemistry department, Faculty of science, Benha University, 13518 Benha, Egypt

ARTICLE INFO

Article history:

Received 12 August 2013

Received in revised form 17 September 2013

Accepted 20 September 2013

Available online 1 October 2013

Keywords:

Nanonickel oxide

Lithium ion batteries

Anode material

Initial discharge capacity

ABSTRACT

Transition metal oxides are extensively investigated as alternative anode materials for lithium ion batteries owing to their high theoretical capacity. In this work, mesoporous nickel oxide nanostructure is synthesized by a simple solution method without high calcination temperature. The sample is characterized using X-ray diffraction, Fourier Transform Infra Red (FT-IR), Scanning Electron Microscopy, Transmission Electron Microscopy, Nitrogen adsorption–desorption isotherm and surface pyridine adsorption. Large surface area, nanosphere particles, mesoporous structure and surface lewis acidic and Brønsted sites are confirmed. The electrochemical properties of mesoporous nanonickel oxide is investigated including the cycling performance as anode material for lithium ion batteries. The results show that nanonickel oxide has a high discharge capacity at 1 C, especially the first 5 cycles, compared to previous studies at low rates (0.035 and 0.14 C) with the same material. Also, nanonickel oxide shows good efficiency through charge–discharge cycles. All results and data are correlated and discussed.

© 2013 Elsevier B.V. All rights reserved.

1. Introduction

Lithium ion batteries (LIBs), a fast-developing technology in electric energy storage, are the dominant power sources for a wide range of portable electronic devices [1–3]. Great efforts are underway to develop new electrode materials and new technologies for next generation of LIBs. Recently, transition metal oxides (such as Co_3O_4 , Fe_3O_4 and NiO) have been extensively investigated as alternative anode materials for LIBs [4–8]. NiO has attracted a considerable attention due to its high theoretical capacity (718 mA h g^{-1}), low cost, natural abundance and environmental friendliness.

It is well known that physical and chemical phenomena can be vastly different in a nanomaterial compared to those observed in its bulk state. This point is clearly illustrated in the transition metal oxide (MO) system ($M = \text{Fe}, \text{Co}, \text{Cu}, \text{Ni}$) by considering the applicability of these materials to Li-ion batteries. In this system, the reaction of the MO with lithium results in the formation of the reduced metal and Lithia (Li_2O). It had long been reported that bulk Li_2O was electrochemically inactive and therefore unable to be decomposed. However, the manufacturing nanostructured MO precursors, the resultant Li_2O is also nanostructured and may be decomposed [4,9] and can allow the reaction of nanostructured MOs with lithium to be made completely reversible and meant that these materials have received significant attention as possible candidates for use in Li-ion batteries.

In this work, we successfully prepared mesoporous nickel oxide nanospheres with large surface area. This material showed us a good initial discharge capacity performance, especially at 1 C rate, with a comparison to recent reported performances of the same material.

2. Experimental work

2.1. Synthesis

Aqueous solutions of NiSO_4 (Fluke, purity 98%) and urea (Merk, purity 99%) were mixed together, adjust pH with diluted ammonia solution to equal 8. Then the above mixture was added into a glass reacting vessel and sealed. The reaction was carried out with magnetic stirring and the temperature was maintained at 95°C . After 6 h., the reaction was stopped by cold water. Finally, alight green sediment was formed. The precipitate was washed with distilled water and acetone for three times, respectively, to remove the possible absorbed ions. After drying at 75°C for 12 h, the precursor was heated in air at 350°C for 1 h to obtain NiO powder with absolute dark color.

2.2. Characterization

X-ray diffraction analysis was performed on a Diano (made by Diano Corporation, USA.) with Cu-filtered $\text{Cu K}\alpha$ radiation ($\lambda = 1.5418 \text{ \AA}$) energized at 45 kV, and 10 mA. The sample was measured at room temperature in the range from $2\theta = 2^\circ$ to 80° . The XRD phases present in the sample were identified with the help of ASTM Powder Data Files.

The infrared spectrum of the sample was recorded in the range of $400\text{--}4000 \text{ cm}^{-1}$ using a Bruker-FTIR. The morphology of sample was examined using field emission scanning electron microscope (SEM, JEOL) and transmission electron microscope (TEM, JEOL-2010) operated at an accelerating voltage of 200 kV.

* Tel.: +20 1203532343.

E-mail address: emad_masoud1981@yahoo.com

The surface acidity was determined by pyridine adsorption. The sample was activated for 1 h at 200 °C, and then exposed to pyridine at room temperature as follows: 2 drops of pyridine were added to 0.1 g of sample and was left to 116 h, and then the adsorbed pyridine was determined using infrared spectroscopy.

Surface area and porosity of the sample was determined by measuring Brunauer–Emmett–Teller (BET) nitrogen adsorption–desorption isotherm using volumetric method with a Micromeritics ASAP2020 apparatus.

2.3. Electrochemical measurements

For setting up the experimental cell, NiO powder (75 wt.%) was mixed with carbon black (10 wt.%), graphite (10 wt.%) and PVDF (5 wt.%) in presence of *n*-methylpyrrolidinone to make the mixture homogeneous and then the mixture was left on a hot plate for 3 h. to evaporate the homogeneity material. After that, a certain weight of the powder was coated onto a copper foil and some drops of *n*-methylpyrrolidinone were added again and then the powder was dried under vacuum for 30 min at 120 °C. In a glove box under argon atmosphere, the cell was constructed as coin-type cells. A porous polypropylene film was used for separating the cathode and a lithium metal anode, and a mixture of 1M LiPF₆-ethylene carbonate/dimethyl carbonate (1:1, v/v, Merck) was used as the electrolyte. The cells were galvanostatically charged and discharged using EG&G Electrochemical analyzer (Model-6310) in the scan rate of 1 mV s⁻¹ to perform charge–discharge processes for the assembled battery. The charge–discharge processes were performed at a voltage between 0 and 3 V and a rate of 1 C.

3. Results and discussions

X-ray diffraction pattern of investigated NiO is shown in Fig. 1. The observed indexed peaks are fully matched with the corresponding pure cubic NiO (JCPDS 47-1049) [10]. The peaks observed in the pattern at $2\theta = 37.1^\circ$, 43.3° and 62.8° are assigned to the (111), (200), and (220) crystal planes, respectively. Moreover, no peaks for any impurities such as α -Ni(OH)₂, β -Ni(OH)₂, or other phases were observed in the pattern. It is well known that, the diffraction peaks are broader and have weaker intensity when the size of particle is decreased to the extent. The average crystallite size of the prepared NiO sample was calculated by Scherrer's Formula [11]

$$d_{XRD} = k\lambda / \beta \cos\theta \quad (1)$$

where k is a shape factor which is taken to be 0.9, λ is the wavelength of X-ray (0.1789 nm), β is the full width at half maximum (FWHM) and θ is the diffraction angle. The obtained crystallite size is found to equal 3 nm.

FT-IR spectrum of nanoNiO is shown in the 4000–400 cm⁻¹ region, Fig. 2. The figure showed a peak appearing at ~422–616 cm⁻¹. It was assigned to the Ni–O stretching of the octahedral NiO groups in the face center cubic [12]. The peaks observed at 3340 and 1645 cm⁻¹ are assigned to the existence of water [13]. Also, the peak observed at 2385 cm⁻¹ is assigned to CO₂ in air [13].

Fig. 3a shows the typical SEM image of nanoNiO. It shows agglomerated nanoparticles with spherical shapes. Usually, spherical shapes are formed because the nucleation rate per unit area is isotopic at the interface between the NiO nanoparticles, which the

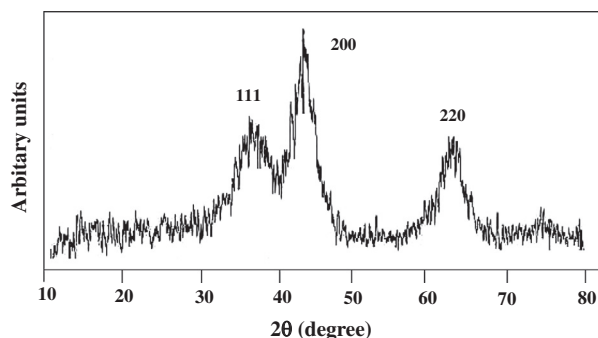


Fig. 1. XRD pattern of nanoNiO.

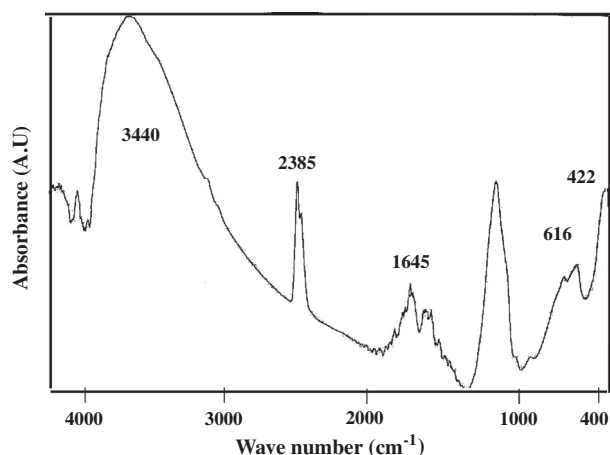


Fig. 2. FT-IR spectrum of nanoNiO.

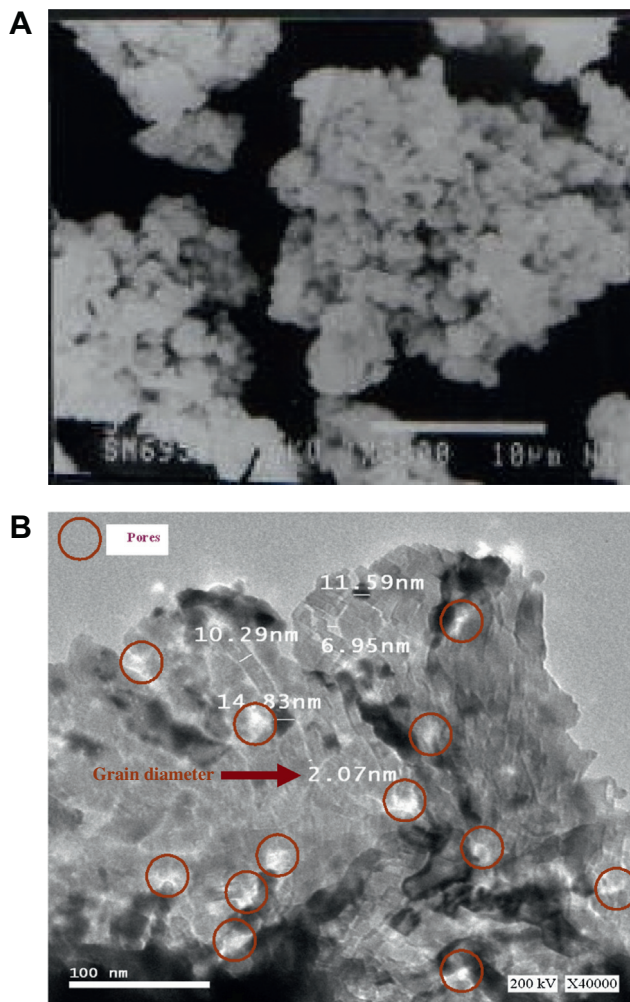


Fig. 3. (a,b) SEM and TEM images of nanoNiO, respectively.

driving forces for Ostwald ripening. This produces a minimization in the surface free energy by the reduction of total surface area/volume, results in the equivalent growth rate along different directions of the nucleation because the sphere has the smallest surface area per unit volume of any shape.

Fig. 3b shows the TEM image of porous nanoNiO. It can be seen that the nanoparticles have different diameters with average value around 5 nm.

The textural properties of nanoNiO sample were further investigated by nitrogen adsorption–desorption isotherm as shown in Fig. 4. The specific surface area was calculated using BET method and found equals $230 \text{ m}^2/\text{g}$. Also, the total pore volume and average pore radius were 0.248 ml/g and 10 nm , respectively.

Fig. 5, V_{ads} against t (thickness in angstrom) plot, reveals the mesoporosity character, as indicated by upward deviation from the initial straight line which passes through the origin. This means a formation of adsorbed multilayer at some pressures argued by capillary condensation in wide pores of the sample.

In order to further investigate the nature of NiO surface, FT-IR spectrum of adsorbed pyridine was performed on nanoNiO at 25°C to investigate the surface sites, Fig. 6. The spectrum displays two main bands. Strong broad bands appearing at 1635 cm^{-1} and 1465 cm^{-1} are indicative for the formation of Brönsted pyridine species (Bpy) and Lewis pyridine (Lpy) ones, respectively [14].

In order to investigate the lithium storage capacities of porous NiO nanospheres, galvanostatic charge/discharge cycling at a current density of 1 C was determined, Fig. 7. The figure showed that the first charge and discharge capacities of nanoNiO have high values of $782.9 \text{ mA h g}^{-1}$ and $1070.3 \text{ mA h g}^{-1}$ at 1 C , respectively. The capacity retention through the first five cycles is good as the value of capacity for charge and discharge is 580 mA h g^{-1} and 600 mA h g^{-1} for the fifth cycle, respectively. This sample with its textural properties has a good performance through the first 5 cycles compared to the previous reported performances of NiO nanospheres [15], NiO hollow microspheres [16] and NiO nanotube [17] that showed a good discharge capacity, but at low current rates ($0.035\text{--}0.14 \text{ C}$), Table 1. A comparison of the electrochemical properties of mesoporous NiO nanospheres with recent studies is shown in Table 1. This means that several factors such as surface area, particle size and structure stability are competing with each other, which may affect the Li-ion storage performance [18–20]. Also, In the previous reports, Zhu et al. summarized that the optimal grain size, crystallinity and morphology codetermined the property of anode material [19]. Yan et al. also reached a similar conclusion and further pointed out that well – crystalline material could maintain the nanocrystallite size and activate the decomposition of Li_2O , thus increasing the discharge capacity [18]. Also, as we all know, the diffusion length for lithium ion and electron is especially important for cycling [15]. The small particle size can reduce the mean Li diffusion pathways and increase the contact surface area between the anode and the electrolyte [21]. These effects can promote faster ionic transport and contribute to faster charge–discharge processes in secondary lithium batteries [22]. Also, it is well known that a large surface area is important for the improvement of reaction performance, in terms of the introduction of lithium ions through the nickel oxide surface. The capacity and affinity will be greatly enhanced when the surface area is high, since the

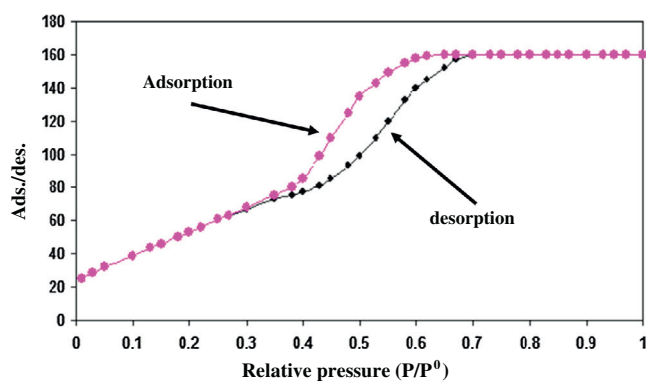


Fig. 4. Adsorption–desorption isotherm of nanoNiO.

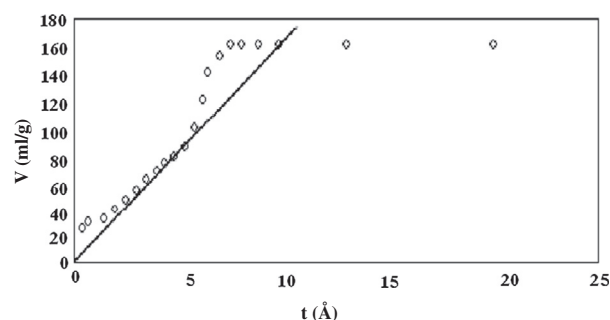


Fig. 5. V - t plot for nanoNiO.

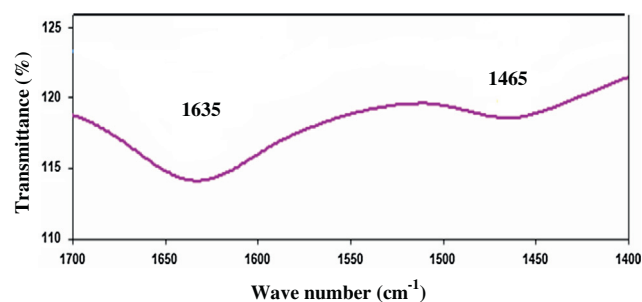


Fig. 6. FT-IR spectrum of adsorbed pyridine on nanoNiO.

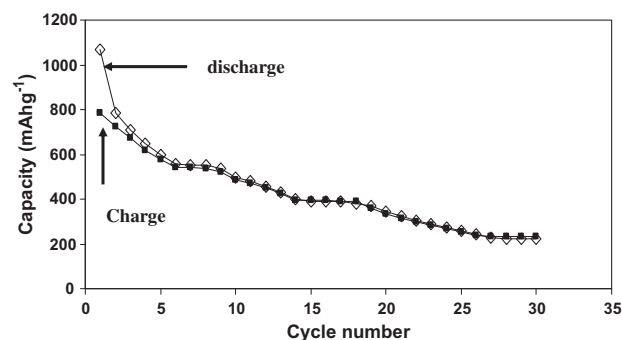


Fig. 7. Charge–discharge capacity against cycle number for nanoNiO sample at 1 C rate.

diffusion lengths of the lithium ions are greatly shortened [23]. Therefore, the materials with the smaller size and highest surface area would exhibit the highest discharge capacity [24].

Moreover, the porous structure with large surface to volume ratio and short diffusion length for lithium intercalation can lead to superior cycling and rate performance of electrode materials [25,26]. For our investigated sample, the mesoporous structure confirmed by TEM and $V_{\text{ads}}-t$ plot provides a space for the volume expansion during lithiation. Moreover, these grains enlarge and adhere together to form a compact layer, which have a high stability and preserve the integrity of the structure.

The porous structure can not only benefit the diffusion of solid state Li-ion [27–31], but also accommodate volume changes of charge/discharge process to maintain the structure integrity [32,33].

This improved cycling at 1 C rate compared to recent performance at low rates can be attributed to the large surface area ($230 \text{ m}^2 \text{ g}^{-1}$), the small particle size (3 nm), and the mesoporous structure [34].

In addition to what mentioned above, the lewis and Brönsted acidic sites confirmed by pyridine adsorption may also participate in improving the interaction of Li ion with nanonickel oxide

Table 1
Comparison of the electrochemical properties of mesoporous nanoNiO.

Sample	Particle size (nm)	Current density (C)	Potential range (V)	Initial capacity (mA h g ⁻¹)	Capacity retention (mA h g ⁻¹)	References
NiO nanosphere	3 nm	1	0–3	1070.3	600 after 5 cycles	This work
NiO nanosphere	5–10 nm	0.14	0–3	1220	900 after 5 cycles	[15]
NiO nanotube	Wall thickness = 20–30 nm	0.035	0.025–3	600	305 after 5 cycles	[17]
NiO hollow microsphere	200 nm	0.14	0–3	700	690 after 5 cycles	[16]

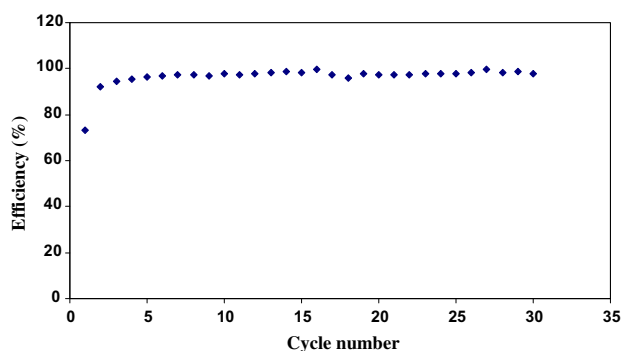


Fig. 8. Cycle number dependence of efficiency for nanoNiO sample.

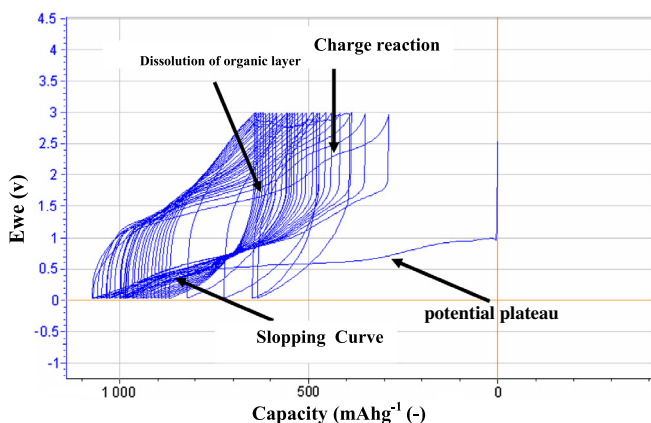


Fig. 9. Galvanostatic lithium insertion/extraction curves of NiO electrode between 0 and 3 V at a current density of 1 C.

surface. This can be discussed as the nanoparticles of NiO gets in contact with their neighbors, to finely form a continuous interpenetrating structure. The positive space charge layer of the individual particles caused by those sites overlap to form a continuous network of favorable diffusion pathways with short length resulting in an improvement of Li interaction with NiO surface through the discharge reaction and as a result showing a good discharge capacity.

At the same time, the efficiency behavior of nanoNiO through charge–discharge processes confirmed that nanoNiO sample has a good efficiency, Fig. 8. It shows that efficiency of the first cycle was 73% and then increased to show almost stable values till the last cycle that showed a value of 98%. The extra capacities are mainly due to the decomposition of non-aqueous electrolyte during the discharge process [35].

Fig. 9 shows the charge–discharge curves for all cycles. It generally shows that charge–discharge curves present similar behaviors. The initial discharge curve shows a clear potential plateau at around 0.6 V followed by a sloping curve, which corresponds to the following reaction [15]:

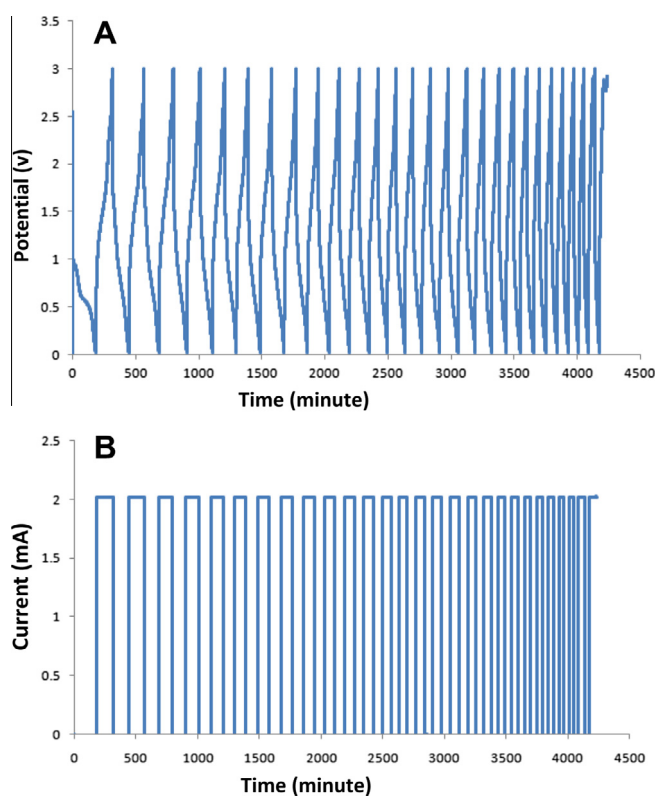


Fig. 10. Time dependence of (A) potential and (B) current for nanoNiO sample.

The slopping part at the end of the discharge curve (between 0.6 and 0 V) is corresponding to the formation of a solid electrolyte interface layer [36,37]. The slop in the other discharge curves is a round 1.4 V.

Also, there are two slops a round 1.6 and 2.3 V in each charge curve which corresponding to the dissolution of the organic solid electrolyte interface layer [35,38] and the charge reaction $\text{Ni} + \text{Li}_2\text{O} \rightarrow \text{Ni} + 2\text{LiO}$ [15], respectively.

Fig. 10a,b shows the charge–discharge voltage and current versus time for NiO/Li cell. The figures reflected the regular and stable behavior for each voltage and current with time for all charge–discharge cycles.

4. Conclusions

Pure NiO was prepared using a solution method without high calcination temperature. The sample was characterized using different techniques like X-ray diffraction, FT-IR, SEM, TEM, nitrogen adsorption–desorption and surface pyridine adsorption. Characterization techniques showed that NiO has pure cubic structure with small particle size (3 nm), nanosphere shape, large surface area (230 m² g⁻¹) with mesoporous structure and Lewis acidic and Brønsted sites. Electrochemical tests at rate of 1 C showed that this sample has a good discharge capacity especially for the first 5 cycles compared to previous recent studies. The sample delivered

initial discharge and charge capacities of 1070.3 and 782.9 mA h g⁻¹, respectively. Also, it showed a good efficiency and regular and stable behavior for each potential and current with time through cycles of charge and discharge. This improved electrochemical behavior at 1 C compared to the previous recent studies at low current rates can be attributed to the large surface area with mesoporous structure and lewis acidic and Brönsted sites.

Acknowledgement

I would like to acknowledge the support provided by the FQM288 research group, UCO University, Spain through a research stay period.

References

- [1] M. Armand, J.M. Tarascon, *Nature* 451 (2008) 652.
- [2] X.L. Sun, X.H. Wang, L. Qiao, D.K. Hu, N. Feng, X.W. Li, Y.Q. Liu, D.Y. He, *Electrochim. Acta* 66 (2012) 204.
- [3] J.S. Chen, L.A. Archer, X.W. Lou, *J. Mater. Chem.* 21 (2011) 9912.
- [4] P. Poizot, S. Laruelle, S. Grugeon, L. Dupont, J.M. Tarascon, *Nature* 407 (2000) 496.
- [5] P.G. Bruce, B. Scrosati, J.M. Tarascon, *Angew. Chem. Int. Ed.* 47 (2008) 2930.
- [6] Y. Li, B. Tan, Y. Wu, *Nano Lett.* 8 (2008) 265.
- [7] C.C. Li, X.M. Yin, Q.H. Li, L.B. Chen, T.H. Wang, *Chem. – A Eur. J.* 17 (2011) 1596.
- [8] W. Xing, F. Li, Z.F. Yan, G.Q. Lu, *J. Power Sources* 134 (2004) 24.
- [9] M.N. Obrovac, R.A. Dunlap, R.J. Sanderson, J.R. Dahn, *J. Electrochem. Soc.* 148 (6) (2001) A576.
- [10] D. Yang, R. Wang, M. He, J. Zhang, Z. Liu, *J. Phys. Chem.* B109 (2005) 7654.
- [11] W.E. Mahmoud, H. El-Mallah, *J. Phys. D: Appl. Phys.* 42 (2009) 035502.
- [12] V. Biju, M. Abdul Khadar, *Spectrochim. Acta, Part A: Mol. Biomol. Spectrosc.* 59 (2003) 124.
- [13] L. Wu, Y. Wu, H. Wei, Y. Shi, C. Hu, *Mater. Lett.* 58 (2004) 2700.
- [14] S. Brunauer, R.Sh. Mikhail, E.E. Bodor, *J. Coll. Inter. Sci.* 24 (1967) 541.
- [15] G. Zhang, Y. Chen, B. Qu, L. Hu, L. Mei, D. Lei, Q. Li, L. Chen, Q. Li, T. Wang, *Electrochim. Acta* 80 (2012) 140.
- [16] X.H. Huang, J.P. Tu, C.Q. Zhang, F. Zhou, *Electrochim. Acta* 55 (2010) 8981.
- [17] S.A. Needham, G.X. Wang, H.K. Liu, *J. Power Sources* 159 (2006) 254.
- [18] N. Yan, L. Hu, Y. Li, Y. Wang, H. Zhong, X.Y. Hu, X.K. Kong, Q.W. Chen, *J. Phys. Chem. C* 116 (2012) 7227.
- [19] J.X. Zhu, Y.K. Sharma, Z.Y. Zeng, X.J. Zhang, M. Srinivasan, S. Mhaisalkar, H. Zhang, H.H. Hng, Q.Y. Yan, *J. Phys. Chem. C* 115 (2011) 8400.
- [20] X.W. Lou, D. Deng, J.Y. Lee, L.A. Archer, *J. Mater. Chem.* 18 (2008) 4397.
- [21] S.H. Choi, J.W. Son, Y.S. Yoon, J. Kim, *Power Sources* 158 (2006) 1419.
- [22] J.M. Tarascon, M. Armand, *Nature* 414 (2001) 359, 456–461.
- [23] Y. Nuli, R. Zeng, P. Zhang, Z. Guo, H. Liu, *Power Sources* 184 (2008).
- [24] S.Y. Zeng, K.B. Tang, T.W. Li, *J. Colloid Interface Sci.* 312 (2007) 513.
- [25] B.H. Qu, M. Zhang, D.L. Lei, Y.P. Zeng, Y.J. Chen, L.B. Chen, Q.H. Li, Y.G. Wang, T.H. Wang, *Nanoscale* 3 (2011) 3646.
- [26] J.T. Zai, X.F. Qian, K.X. Wang, C. Yu, L.Q. Tao, Y.L. Xiao, J.S. Chen, *CrystEngComm* 14 (2012) 1364.
- [27] B.Q. Liu, Q.F. Li, B. Zhang, Y.L. Cui, H.F. Chen, G.N. Chen, D.P. Tang, *Nanoscale* 3 (2011) 2220.
- [28] D.W. Liu, B.B. Garcia, Q.F. Zhang, Q. Guo, Y.H. Zhang, S. Sepehri, G.Z. Cao, *Adv. Funct. Mater.* 19 (2009) 1015.
- [29] C.M. Park, J.K. Jeon, *Chem. Commun.* 47 (2011) 2122.
- [30] X.W. Lou, D. Deng, J.Y. Lee, L.A. Archer, *Chem. Mater.* 20 (2008) 6562.
- [31] H.S. Zhou, D.L. Li, M. Hibino, I. Honma, *Angew. Chem. Int. Ed.* 44 (2005) 797.
- [32] S.M. Yuan, J.X. Li, L.T. Yang, L.W. Su, L. Liu, Z. Zhou, *Appl. Mater. Interfaces* 3 (2011) 705.
- [33] C. Burda, X.B. Chen, R. Narayanan, M.A. El-sayed, *Chem. Rev.* 105 (2005) 1025.
- [34] Y. Liu, X.G. Zhang, *Electrochim. Acta* 54 (2009) 4180.
- [35] S. Grugeon, S. Laruelle, R. Herrera – Urbina, L. Dupont, P. Poizot, J.M. Tarascon, *J. Electrochem. Soc.* 148 (2001) A285.
- [36] H. Liu, G.X. Wang, J. Liu, S.Z. Qiao, H. Ahn, *J. Mater. Chem.* 21 (2011) 3046.
- [37] T. Kavitha, H. Yuvaraj, *J. Mater. Chem.* 21 (2011) 15686.
- [38] A. Debart, L. Dupont, P. Poizot, J.-B. Leriche, J.M. Tarascon, *J. Electrochem. Soc.* 148 (2001) A1266.